Savvas Gkantonas[1]
Department of Engineering,
University of Cambridge,
Trumpington Street,
Cambridge CB2 1PZ, UK
e-mail: sg834@cam.ac.uk

Sandeep Jella
Siemens Energy Canada Ltd,
9545 Côte-de-Liesse Road,
Montréal, QC H9P 1A5, Canada

Salvatore Iavarone
Department of Engineering,
University of Cambridge,
Trumpington Street,
Cambridge CB2 1PZ, UK;
Aero-Thermo-Mechanics Laboratory,
École polytechnique de Bruxelles,
Université Libre de Bruxelles,
Avenue F. D. Roosevelt 50,
Brussels 1050, Belgium

Philippe Versailles
Siemens Energy Canada Ltd,
9545 Côte-de-Liesse Road,
Montréal, QC H9P 1A5, Canada

Epaminondas Mastorakos
Department of Engineering,
University of Cambridge,
Trumpington Street,
Cambridge CB2 1PZ, UK

Gilles Bourque
Siemens Energy Canada Ltd,
9545 Côte-de-Liesse Road,
Montréal, QC H9P 1A5, Canada

Estimation of Autoignition Propensity in Aeroderivative Gas Turbine Premixers Using Incompletely Stirred Reactor Network Modeling

The study of autoignition propensity in premixers for gas turbines is critical for their safe operation and design. Although premixers can be analyzed using reacting computational fluid dynamics (CFD) coupled with detailed autoignition chemical kinetics, it is essential to also develop methods with lower computational cost to be able to explore more geometries and operating conditions during the design process. This paper presents such an approach based on incompletely stirred reactor network (ISRN) modeling. This method uses a CFD solution of a nonreacting flow and subsequently estimates the spatial evolution of reacting scalars such as autoignition precursors and temperature conditioned on the mixture fraction, which is used to quantify autoignition propensity. The approach is intended as a "postprocessing" step, enabling the use of very complex chemical mechanisms and the study of many operating conditions. For a representative premixer of an aeroderivative gas turbine, results show that autoignition propensity can be reproduced with ISRN at highly reactive operating conditions featuring multi-stage autoignition of a dual fuel mixture. The ISRN computations are consequently analyzed to explore the evolution of reacting scalars and propose some autoignition metrics that combine mixing and chemical reaction to assist the design of premixers.
[DOI: 10.1115/1.4055273]

1 Introduction

The safe operation of premixed gas turbine combustors necessitates a thorough understanding of autoignition propensity within the engine premixer, especially as a transition is expected from conventional to next-generation fuels, targeted explicitly for carbon reduction. From the design stage, the reactivity of the fuel-air mixture must be evaluated at engine-relevant conditions with variable levels of preheating and compression ratios, and autoignition risk must be assessed within realistic premixer geometries numerically or experimentally. Premixer design is usually effectuated by an appropriate choice of residence time, long enough to ensure adequate mixing and good combustor operability but significantly shorter than typical ignition delay times to avoid autoignition [1,2]. However, the formation of autoignition kernels and subsequent flame growth and stabilization can still occur at these short time scales, which are all highly linked to the interplay between chemical kinetics and mixing in the formation of autoignition precursors [3].

Computational fluid dynamics (CFD) simulations may be employed to investigate the formation of autoignition precursors and assess the probability of autoignition kernel formation within each premixer, as previously performed for representative premixer geometries [1] or academic configurations (e.g., see Refs. [3,4]). However, careful evaluation of autoignition requires a detailed treatment of turbulent mixing, finite-rate chemistry effects, and the multitude of reaction pathways responsible for precursor formation [5], which raises the overall computational cost, especially when a large number of conditions and geometries have to be evaluated. The latter becomes even more evident when perturbations to operating conditions have also to be considered so that the probability of rare autoignition events can be quantified (e.g., see Ref. [6]) and an engine can be assessed with the whole life cycle operation in mind. As a result, it is essential to develop new methods able to provide a fast and reasonably accurate prediction of autoignition propensity within premixers.

This work presents a methodology based on incompletely stirred reactor network (ISRN) modeling that simplifies such calculations whilst retaining an elaborate treatment of transport, micromixing, and finite-rate chemistry effects on autoignition without sacrificing geometric complexity. The approach relies on an existing CFD solution of the inert flow that is then kinetically postprocessed by solving equations for reacting scalars, such as autoignition precursors and temperature so that autoignition metrics can be explicitly analyzed. The approach may be viewed as an improvement over current chemical reactor network approaches that consider only ideal reactors (e.g., see Refs. [7–9]) by the inclusion of mixture inhomogeneity.

An ISRN constitutes a network of ISRs, defined as flow regions within which conditional averages of reacting scalars, conditioned on a mixture fraction that denotes fuel–air mixing, are homogeneous but with the flow and mixture fraction being inhomogeneous

[1]Corresponding author.

Manuscript received July 11, 2022; final manuscript received July 16, 2022; published online September 2, 2022. Editor: Jerzy T. Sawicki.

[10,11]. The latter are directly considered in the ISRN equations through the mixture fraction probability density function and the scalar dissipation rate, extracted from a CFD computation. For autoignition calculations, density changes are minor before autoignition occurs, so that using only the nonreacting flow and mixing patterns from CFD introduces only small errors. Decoupling the solution of these fields from the solution of reacting scalars reduces the computational time drastically. Furthermore, it allows for the use of chemical mechanisms of arbitrary complexity or the exploration of a broad range of operating conditions, which may prove indispensable to the design engineer focusing on autoignition propensity.

The ISR theory was first developed by Bilger and coworkers [12–15] on the theoretical foundation laid by the conditional moment closure (CMC) method for turbulent reacting flows [16], which has been extensively validated for autoignition problems (e.g., see Ref. [3] and references therein). Methods based on ISRs have previously been applied to experimental lab-scale combustors [14,17], a heavy-duty diesel engine [18], and model aero-engine combustors [10,11,19,20] demonstrating good accuracy for predicting gas-phase pollutants and soot. As opposed to a single ISR, the use of an ISRN introduced first for soot modeling [11] allows for better control of the spatial resolution that can be extracted from the computations since ISRs can be allocated at will in various regions of the flow that exhibit different micromixing rates and residence time distributions. With a focus on statistically-steady conditions, the same principles can be used for the problem of autoignition, as demonstrated by Iavarone et al. [21,22] who validated the ISRN paradigm for autoignition by reproducing the trends of hydrogen autoignition location in a turbulent atmospheric coflow of heated air [23,24]. After selecting an appropriate mixing field and chemical mechanism, the ISRN equations can be solved for a range of operating conditions and the statistically-steady behavior of autoignition location and propensity can be analyzed, e.g., as per the temperature or precursor formation. This type of analysis forms the main subject of this work and examines the ISRN applicability in capturing the autoignition behavior inside an aeroderivative gas turbine premixer previously studied with reacting CFD [1].

The specific objectives of the work are to (i) present the ISRN approach as a method to evaluate autoignition propensity in aeroderivative gas turbine premixers; (ii) to assess the performance in an experimental premixer with real-life geometric complexity; (iii) to study the effects of fuel mixture composition and air temperature on multi-stage autoignition. The paper is structured as follows. The derivation of the ISRN equations is first presented, followed by the description of the solution strategy and the models used in the computations. This is followed by a brief description of the investigated premixer and the mixing field obtained by the reference CFD simulation. Results and key conclusions close the paper.

2 The Incompletely Stirred Reactor Network Approach

The governing equation for an incompletely stirred reactor (ISR), either as a single reactor or as part of a reactor network (ISRN), may be viewed as a spatially integrated approximation of the CMC equation, analyzed in various works (e.g., see Refs. [11,16]). An ISR is considered to be a core volume V within which conditional averages of reacting scalars, with the conditioning variable being the mixture fraction, are independent of position and time. Unlike a perfectly stirred reactor, which has uniform composition, this allows an ISR to have flow and mixture fraction inhomogeneities.

2.1 Mathematical Model. The derivation leading to the ISRN governing equations has been presented previously in Refs. [10,11,19,20], but is also presented here for completeness. It is based on the transport equation of the conditional expectation (here considered to be density-weighted and time-averaged) of a generic species α, $Q_\alpha \equiv \langle Y_\alpha|\xi=\eta\rangle$, but also includes the mixture fraction PDF, P_η, with η being the sample space variable of the mixture fraction, ξ. Following [16], the transport equation reads

$$\frac{\partial \bar{\rho} Q_\alpha P_\eta}{\partial t} + \nabla\cdot\left(\bar{\rho}\langle \mathbf{u}Y_\alpha|\eta\rangle P_\eta\right) = -Q_\alpha \frac{\partial^2 \bar{\rho}\langle N|\eta\rangle P_\eta}{\partial \eta^2} + \bar{\rho}\langle N|\eta\rangle P_\eta \frac{\partial^2 Q_\alpha}{\partial \eta^2} + \bar{\rho}\langle \dot{\omega}_\alpha|\eta\rangle P_\eta \tag{1}$$

where $N \equiv D\nabla\xi\cdot\nabla\xi$ is the scalar dissipation rate (SDR) and $\langle\dot{\omega}_\alpha|\eta\rangle$ a chemistry source term. Note that a unity Lewis number assumption has been employed in Eq. (1). Differential diffusion effects can be included (e.g., see Ref. [11] for an overview), but this is not necessary for the hydrocarbon fuels considered in this work; hence they have been omitted. Considering statistically stationary flow, the integration of Eq. (1) over the core volume and the application of the flux divergence theorem to the left-hand side leads to

$$\oint_A \bar{\rho}\langle \mathbf{u}Y_\alpha|\eta\rangle P_\eta\cdot d\mathbf{A} = -\int_V \left(Q_\alpha \frac{\partial^2 \bar{\rho}\langle N|\eta\rangle P_\eta}{\partial\eta^2}\right) dV + \int_V \left(\bar{\rho}\langle N|\eta\rangle P_\eta \frac{\partial^2 Q_\alpha}{\partial\eta^2} + \bar{\rho}\langle\dot{\omega}_\alpha|\eta\rangle P_\eta\right) dV \tag{2}$$

In ISR theory [16], conditional correlations between reacting scalars and velocity are neglected, but they are retained in Eq. (2), as they may be of the same magnitude with convective fluxes between interconnecting ISRs. These are closed with a diffusion approximation [16], assuming a time-averaged turbulent diffusivity, D_T, which can incorporate both large-scale and small-scale turbulent flux contributions. A method of how D_T can be computed will be given later. By definition, conditional reactive scalar statistics and their functions, e.g., chemical source terms, are considered uniform inside an ISR core. Hence, they can be moved out of the integral on the RHS of Eq. (2). This allows for the introduction of the core-averaged mass density, ρ^{**}, mixture fraction PDF, P_η^{**}, and SDR, N_η^{**}, in the equation, which can be computed by CFD simulations after appropriate time-averaging. The core-averaged quantities are given by:

$$\rho^{**} \equiv \frac{\int_V \bar{\rho} dV'}{V};\quad P_\eta^{**} \equiv \frac{\int_V \bar{\rho} P_\eta dV'}{\rho^{**}V};\quad N_\eta^{**} \equiv \frac{\int_V \bar{\rho}\langle N|\eta\rangle P_\eta dV'}{\rho^{**}VP_\eta^{**}} \tag{3}$$

Moreover, conditional statistics are only a function of mixture fraction. Therefore, their partial derivatives may be transformed into ordinary ones. The governing equation can then be written in the following discrete form:

$$\sum_{i=1}^{\mathcal{F}^{\text{out}}}(\dot{m}P_\eta Q_\alpha)_i - \sum_{j=1}^{\mathcal{F}^{\text{in}}}(\dot{m}P_\eta Q_\alpha)_j - \sum_{i=1}^{\mathcal{F}}(\bar{\rho}P_\eta D_T\mathbf{A}\cdot\nabla Q_\alpha)_i = \rho^{**}V\left(P_\eta^{**}\left(N_\eta^{**}\frac{d^2Q_\alpha}{d\eta^2} + \langle\dot{\omega}_\alpha|\eta\rangle\right) - Q_\alpha\frac{d^2N_\eta^{**}P_\eta^{**}}{d\eta^2}\right) \tag{4}$$

where $\dot{m}$ the mass flow rate passes through a particular face (with an index ranging from 1 to $\mathcal{F}$) at the inlet or outlet streams of an ISR. In the limit of a single inlet and outlet stream face, the reactor residence time could be defined as $\tau_r \equiv (\rho^{**}V)/\dot{m}$. Note that a conditional independence model has also been assumed for the

conditional velocity, i.e., $\langle \mathbf{u}|\eta \rangle = \mathbf{u}$, simplifying the mass flow rate definition appearing in Eq. (4). In the context of CMC, minor differences have been observed between different models for the conditional velocity [25] using a time-averaged approach; hence the differences are also expected to be small here.

To close the first term on the RHS of Eq. (4) the transport equation for the mixture fraction PDF may be utilized [16]. If molecular fluxes are neglected, the PDF equation is equivalent to Eqs. (1) and (4) with $Q_\alpha = 1$ and no chemistry source term. Since Q_α is constant, its derivative is zero. Given a statistically stationary flow, the PDF equation can be written in discrete form as in

$$\sum_{i=1}^{\mathcal{F}^{\text{out}}} (\dot{m}P_\eta)_i - \sum_{j=1}^{\mathcal{F}^{\text{in}}} (\dot{m}P_\eta)_j = -\rho^{**} V \frac{d^2 N_\eta^{**} P_\eta^{**}}{d\eta^2} \tag{5}$$

Consistently with the stirred reactor concept, the conditional quantities exiting an ISR must be taken equal to conditional quantities in the core, hence $(Q_\alpha)_i = Q_\alpha, \forall i = [1, \mathcal{F}^{\text{out}}]$. As discussed in Ref. [15], this is a requirement to allow the solution of the governing equations. Finally, the combination of Eqs. (4) and (5) leads to the governing equation of an ISRN element:

$$\underbrace{\sum_{j=1}^{\mathcal{F}^{\text{in}}} \frac{(\dot{m}P_\eta)_j}{\rho^{**} V P_\eta^{**}} \left[Q_\alpha - (Q_\alpha)_j\right]}_{\mathcal{T}_1 - \text{advection flux}} - \underbrace{\sum_{i=1}^{\mathcal{F}} \frac{(\bar{\rho} P_\eta D_T \mathbf{A} \cdot \nabla Q_\alpha)_i}{\rho^{**} V P_\eta^{**}}}_{\mathcal{T}_2 - \text{turbulent flux}} = \underbrace{N_\eta^{**} \frac{d^2 Q_\alpha}{d\eta^2}}_{\mathcal{T}_3 - \text{micromixing}} + \underbrace{\langle \dot{\omega}_\alpha | \eta \rangle}_{\mathcal{T}_4 - \text{source}} \tag{6}$$

Equation (6) consists of four terms that incorporate effects of advection fluxes ($\mathcal{T}_1$), turbulent fluxes ($\mathcal{T}_2$), micromixing ($\mathcal{T}_3$), and chemistry sources ($\mathcal{T}_4$). In the absence of terms $\mathcal{T}_1$ and $\mathcal{T}_2$, Eq. (6) is virtually identical to the steady-state flamelet model for unity Lewis number, whereas in the special case of $\mathcal{F}^{\text{in}} = 1$ and $D_T = 0$, the governing equation for a single ISR (describing a flow system in its entirety [6,15,16]) is restored. Here, the governing equation for the mass fraction of a generic species was only shown, but an equation for the conditional absolute specific enthalpy must also be solved. It is written similarly to Eq. (6) with the source term containing only heat losses, e.g., radiative or convective losses to walls.

2.2 Solution Strategy. The solution strategy of the ISRN approach for autoignition propensity evaluations is summarized in Fig. 1. The approach starts with creating a standard computational grid and the calculation of the average nonreacting flow field using CFD. The ISRN equations must then be solved, which was here achieved via an in-house unstructured finite volume parallel code, initially developed for CMC modeling (e.g., see Ref. [11] and references therein). The evaluation of fluxes and core-averaged quantities (see "Preprocessor" in Fig. 1) requires knowledge of the mean flow and mixing fields from the CFD calculation and information about the CFD grid topology and connectivity. As discussed in Ref. [10], the modeling approach for the reference CFD simulation can vary given the availability of resources, but care must be taken for each specific application so that the underlying mixing field is well captured. In this work, a nonreacting large eddy simulation (LES) simulation was used which is described in more detail later.

The reactor network is reconstructed around the CFD grid by exploiting the grid topology. After providing the ISR centroids, simply as a "desired" list of Cartesian coordinates, the individual reactor volumes are obtained through an agglomeration of CFD cells based on the minimum distance between cells and centroids. This allows for arbitrary ISR spacing and directly conserves the mass fluxes computed at the CFD resolution. In contrast with ideal

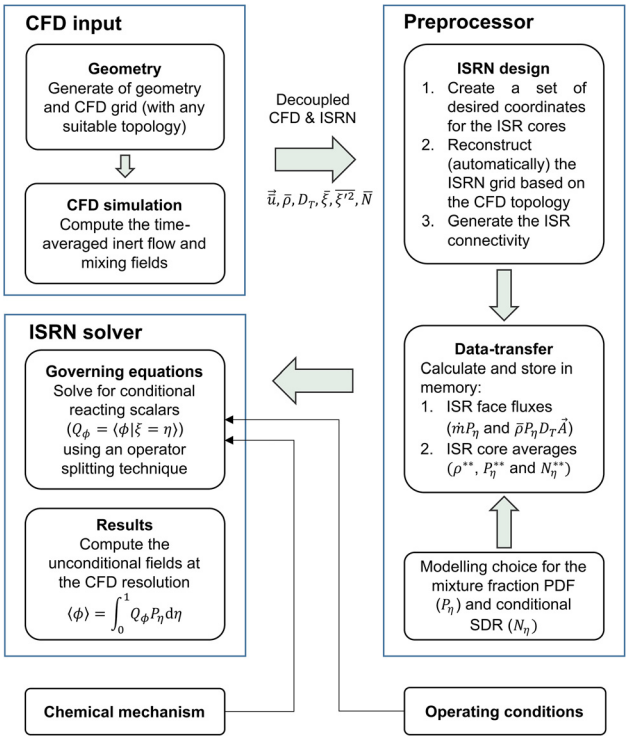

Fig. 1 Incompletely stirred reactor network (ISRN) solution strategy for autoignition propensity evaluations

reactor network approaches, clustering procedures are not required to identify chemically and physically homogeneous zones since ISRs are inhomogeneous in terms of their flow and mixture fraction fields. However, regions of the flow may be discarded if necessary to speed up computations and reduce memory usage. For example, these could be flow regions with pure air or fuel where autoignition is impossible. The ISR spacing and design employed in this study will be presented in Sec. 3.

CFD-derived quantities are then evaluated at the faces of ISR reactors to precompute and store averages over the ISR core volume (see Eq. (3)) or parts of the advection ($\mathcal{T}_1$) and turbulent flux terms ($\mathcal{T}_2$) of Eq. (6). At this point, the mixture fraction PDF, P_η, and the turbulent diffusivity, D_T, must be modeled and evaluated at the CFD resolution. Here, the mixture fraction PDF is modeled with a presumed β-function computed from the time-averaged mixture fraction and mixture fraction variance, which are readily available from the simulation. In the case of singularities, the β-function is replaced or complemented by δ-functions. In Eq. (6), it is evident that the division with the core-averaged PDF can lead to numerical problems when the PDF tends to zero. To ensure that the fluxes $\mathcal{T}_1$ and $\mathcal{T}_2$ do not take unrealistically high values, the division with the PDF can be approximated by $1/P_\eta^{**} \approx P_\eta^{**}/(P_\eta^{**2} + \epsilon_P^2)$, where ϵ_P an absolute tolerance for the core-averaged PDF (here $\epsilon_P = 10^{-8}$). An excessive ratio between $(P_\eta)_j$ (at the j-th face of an ISR) and P_η^{**} (at the core) may also result in numerical problems at locations of non-negligible probability but was here kept below a value of 20 at all times by appropriately adapting the ISRN design.

The turbulent diffusivity, D_T, is usually available from the modeling of the mean mixture fraction, for example, in a RANS computation. However, in LES, D_T is not available, so it has to be approximated by including the contribution of both resolved and sub-grid scales. These contributions may be taken from a time-averaged resolved mixture fraction flux $\langle \tilde{\mathbf{u}} \tilde{\xi} \rangle$ and a sub-grid scale mixture fraction flux vector $\langle D_{\text{sgs}} \nabla \tilde{\xi} \rangle$ with D_{sgs} being a sub-grid scale diffusivity typically available from the modeling of the resolved mixture fraction. The above can then be combined to estimate D_T using a diffusion approximation formula for the

unconditional covariance $\langle u'\xi' \rangle$, as in $D_T \approx (||\langle \tilde{\mathbf{u}}\tilde{\xi}\rangle - \langle \tilde{\mathbf{u}}\rangle\langle\tilde{\xi}\rangle - \langle D_{sgs}\nabla\tilde{\xi}\rangle||)/||\nabla\langle\tilde{\xi}\rangle||$. Note that $\tilde{\xi}$ refers to the time-averaged mixture fraction. It is important to ensure that D_T decays to zero when $||\nabla\langle\tilde{\xi}\rangle|| \to 0$, therefore an absolute tolerance ϵ_D (here $\epsilon_D = 10^{-8}$) is applied to the division similar to how ϵ_P is used for the core-averaged PDF.

The conditional scalar dissipation rate (SDR) is modeled and evaluated at the CFD level to compute its core-averaged conditional counterpart, N_η^{**}, appearing in Eq. (6) (see term $\mathcal{T}_3$). For this purpose, the amplitude mapping closure model [26] is employed, i.e., $\langle N|\eta\rangle = N_0 G_\eta$ where G_η and N_0 are $G_\eta = \exp(-2[\text{erf}^{-1}(2\eta-1)]^2)$ and $N_0 = \bar{N}/\int_0^1 P_\eta G_\eta d\eta$. The time-averaged unconditional SDR, $\bar{N}$, may be directly extracted from the CFD simulation. An alternative approach to compute N_η^{**} is to directly use Eq. (5) after a double integration, similar to what is typically attempted in single ISR approaches (e.g., see Refs. [4,6,15]). However, the double integration can prove cumbersome when the PDF tends to zero [16]. Realisability problems could potentially be solved using the methods of Refs. [27,28], as attempted by Iavarone et al. [21,22] for the ISRN computation of a canonical hydrogen plume within a turbulent coflow of heated air. Nevertheless, here the more robust approach of modeling the SDR was preferred because it can ensure realisability for any choice of ISRN design and for any premixer, where regions with very low probability and steep gradients of the mixture fraction PDF are typically expected.

Mixture fraction space is discretized using 101 nodes clustered around the stoichiometric mixture fraction. Care was taken in the resolution around the most-reactive mixture fraction [3], which will be described later. Pure air with temperature T_{ox} is imposed at the $\eta = 0$ boundary, whereas the fuel composition at temperature T_f (smaller than T_{ox}) is imposed at $\eta = 1$. The pressure is assumed constant and equal to the nominal operating pressure of the premixer. The system is assumed adiabatic; therefore, the conditional enthalpy remains constant throughout the computation and the conditional temperature may be identified via a reverse calculation (here with an absolute tolerance of 10^{-8}). All simulations are initialized from an inert mixing solution that is also imposed at the premixer inlet. A zero-gradient condition is imposed at the premixer walls and the outlet for all reacting scalars.

An operator splitting technique is implemented for the solution of the ISRN equations, which are marched in time until convergence is reached. Transport in physical space, i.e., terms $\mathcal{T}_1$ and $\mathcal{T}_2$ of Eq. (6), is solved first, followed by micromixing ($\mathcal{T}_3$) and the integration of the chemistry ($\mathcal{T}_4$) employing the chemical mechanism by Jella et al. [1] and first-order moment closure [16]. For term $\mathcal{T}_4$, the SpeedCHEM solver was employed which significantly speeds up computations by exploiting a sparse analytical Jacobian formulation. The effect of the operator splitting between diffusion and chemistry has been assessed at steady-state with the amplitude mapping closure model for the conditional SDR profile and no transport in physical space. The results were then compared with the method of lines finding negligible differences for temperature, major species, and radicals for pseudo-time steps below 2 μs and values smaller than 10^{-4} and 10^{-16} for relative and absolute internal tolerances in the chemistry solver (e.g., see Ref. [29] for a similar assessment applied to the elliptic CMC equation). A constant pseudo-time-step of 1 μs is used here. A first-order upwind scheme is used to evaluate conditional gradients, whereas the diffusion term in mixture fraction space is discretized with a second-order scheme.

At the end of an ISRN simulation, unconditional quantities may be computed through integration with the mixture fraction PDF. In particular, the unconditional mean of a scalar ϕ is given by

$$\langle\phi\rangle = \int_0^1 Q_\phi P_\eta d\eta \tag{7}$$

with P_η being the mixture fraction PDF at the CFD level and Q_ϕ being the conditional mean of the ISR that contains the particular CFD cell under investigation. Furthermore, unconditional values are here calculated after applying an inverse square distance interpolation to find Q_ϕ over neighbor ISR reactors. Mastorakos [3] discusses the importance of carefully conducting numerical analyses of autoignition since small errors in the calculation of intermediate species and precursors can lead to significant discrepancies in autoignition behavior, even in simple canonical configurations. With this in mind, additional computations (not shown here) were conducted to study the sensitivity to the numerical parameters used in each submodel and numerical solver as applied to the investigated premixer. Our analysis confirmed the past experience but indicated an optimal parameter set beyond which autoignition propensity does not change appreciably for a given ISR spacing. This parameter set is employed here; however, it should be applied judiciously to other flows.

3 Investigated Premixer and Computational Fluid Dynamics Analysis

An experimental premixer is investigated here to demonstrate the ISRN modeling framework. The same premixer was studied previously by Jella et al. using reacting CFD [1]. The premixer, engineered to have a characteristic residence time approximately six times shorter than the worst-case autoignition delay of typical natural gas, features multiple jets injecting pure air into a cross stream of gaseous fuel in the form of a film [1]. The distributed injection of air and fuel results in a range of residence times that also significantly damps thermoacoustics for a wide range of operating conditions [2].

A representation of the mean flow and mixing fields obtained with nonreacting LES is shown in Fig. 2. The Favre-filtered continuity and momentum equations, as well as transport equations for the mixture fraction, $\tilde{\xi}$, and its sub-grid scale variance, $\tilde{\xi''^2}$, were solved using the STAR-CCM+ CFD software. The Wall-Adaptive Large Eddy Simulation (WALE) model of Nicoud and Ducros [30] was used to model sub-grid stresses. The filtered scalar dissipation rate, $\tilde{N}$, used in the sub-grid scale variance transport equation, was computed considering both the resolved and sub-grid scale contributions [31,32] as in $\tilde{N} = D\nabla\tilde{\xi}\cdot\nabla\tilde{\xi} + C_N\tilde{\xi''^2}\mu_{sgs}/(2\rho\Delta^2)$, where $C_N = 42$ [33,34], μ_{sgs} the sub-grid scale viscosity and Δ the filter width estimated as the cube root of the LES cell volume. The molecular diffusivity was calculated from the kinematic viscosity of the mixture using a constant Schmidt number ($Sc = 0.7$). A bounded central differencing scheme was employed for the convective terms in the momentum equation while the diffusion terms were discretized using pure central differencing. Second-order upwinding was used for all scalars. The temporal terms were discretized using an implicit second-order backward differencing scheme, and a time-step restricting the CFL number to less than 0.5 was chosen. The mesh cell size in the premixer was 0.2 mm or smaller.

The CFD simulation was set at representative full load conditions. These were chosen as the combination of preheat, pressure, and stoichiometry represents a highly reactive operating condition. In addition, the fuel mixture composition is also of critical importance. In service, the engine is operated with natural gas. However, a blend of highly reactive gaseous dimethyl ether (DME) fuel with the chemical formula CH_3OCH_3 and less reactive methane (CH_4) gas is used in this experimental premixer to increase the frequency of autoignition events [1]. As discussed by Jella et al. [1], DME-blended methane can be used to test the robustness of high-pressure premixers to autoignition and model the effect of higher hydrocarbons in natural gas. The CFD simulation considered a fuel mixture of pure CH_4 with 40% (v/v) DME. As will be explained later, the fuel composition and the temperature of the (oxidizer) air stream are modified in the ISRN computations but considering the same underlying mixing field: the deviations are deemed small enough to cause limited differences in velocity and density and,

consequently, the changes in the mixture fraction distribution are negligible.

A detailed CFD analysis on this premixer has already been provided by Jella et al. [1], so only a brief summary is provided here. A similar analysis to the one provided here may also be found in Ref. [6]. Figure 2 shows the normalized mean velocity magnitude and mean scalar dissipation rate (SDR) fields in a section of the premixer, as computed from the nonreacting simulation. The presence of the air jets can be inferred by the red "spots" in the mean velocity field in the upstream region, indicating high velocity. Each red spot is also associated with a wake on the lee side that affects the local residence time and mixing rate. The flow decelerates between the last row of air jets and the guide vane and is then quickly accelerated on its way to the vane's trailing edge and toward the premixer exit. Until the flow reaches the premixer exit, the mixing intensity is low, and the mixture fraction has attained the well-mixed value closely, as can be indicated by the overall very low SDR values in the downstream region of Fig. 2. Most of the mixing occurs near the fuel injection region, where the SDR is very high (not shown). Toward the last rows of air jets, the scalar dissipation rate obtains moderate values but can still span several orders in magnitude depending on the location relative to the air jets, until a significant decay is observed soon after the last row or air jets.

Information regarding the mixing field can also be obtained through the mixture fraction PDF. Figure 3 shows the profile of P_η^{**} as a function of η, i.e., the sample space variable for the mixture fraction, up to a reference mixture fraction, η_0, considering a location close to the premixer exit (dashed–dotted line) and two locations in the air jets region. Here, ISRs are considered to be positioned along the flow direction so that P_η^{**} corresponds at cross-stream (mass-weighted) averages at the premixer exit and the air jets region. Two peaks are overall evident in the PDF profiles of the air jets region, one at $\eta = 0$ corresponding to the air stream and another at the well-mixed mixture fraction, here denoted as $\xi_{\text{mixed}} = 1/(1 + \dot{m}_{\text{ox}}/\dot{m}_{\text{f}})$ with $\dot{m}_{\text{ox}}$ and $\dot{m}_{\text{f}}$ being the oxidizer and fuel mass flow rates. In reality, the PDF profiles are tri-modal since another peak is present at $\eta = 1$ corresponding to the fuel stream (not shown). As mixing occurs, the PDF profile tends to a single-peak profile, centered around ξ_{mixed}. The local distribution and the width around ξ_{mixed} are a measure of the unmixedness within the premixer, which may also be evaluated using the whole premixer volume for the average PDF (see solid line). At the same time, the PDFs indicate the extent to which the stoichiometric, ξ_{st}, and the most reactive (as defined by Mastorakos [3]), ξ_{mr}, mixture fractions are present in the premixer at both the large and small scales.

The most reactive mixture fraction, ξ_{mr}, corresponds to the location of the first autoignition kernel in mixture fraction space in the absence of hydrodynamic stretch [3]. Figure 3 shows the

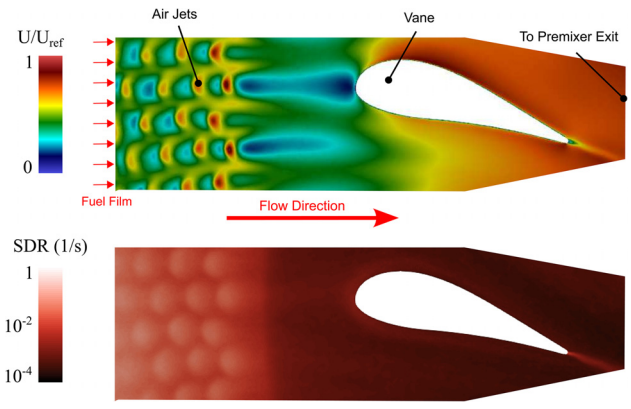

Fig. 2 Normalized mean velocity magnitude field (top) and mean scalar dissipation rate in a section of the investigated premixer (bottom)

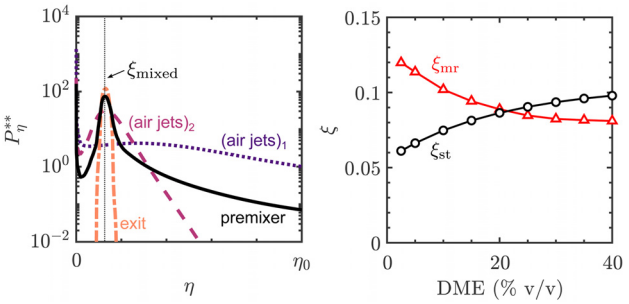

Fig. 3 Left: mixture fraction PDFs at three characteristic locations and from the whole premixer volume of the CFD solution, with the well-mixed mixture fraction indicated by the dashed line. Right: stoichiometric and most reactive mixture fraction as a function of the amount of DME in the fuel for the reference temperatures, the latter obtained from separate homogeneous mixture calculations following the initialization procedure of Ref. [3].

dependency of ξ_{st} and ξ_{mr} with increasing level of DME at the reference operating condition. The premixer's target equivalence ratio is overall fuel-lean with ξ_{mixed} being significantly smaller than ξ_{st} and ξ_{mr} in all cases. It is evident that up to about 20% (v/v) DME in the fuel, the first autoignition kernel is more likely to occur in fuel-rich zones, whereas for higher DME levels, autoignition is more likely in fuel-lean zones. With different operating conditions, ξ_{st} and ξ_{mr} differ but so is the probability of finding these mixture fractions in the premixer. These observations are important for the remainder of the discussion.

Once the time-averaged inert flow field is available, the ISRN approach is applied to the experimental premixer with the main objective to solve Eq. (6) in a postprocessing fashion using different levels of DME in the fuel and different oxidizer (air) temperatures. For the latter, the reference temperature $T_{\text{ox,ref}}$ corresponds to the oxidizer temperature at full load. For this study, the simulation domain is partitioned in ~300 ISRs, uniformly positioned along the flow direction (see Fig. 2). As explained in Refs. [10,11,35], the ISR spacing should be designed to adequately resolve the gradients of conditional quantities within the various flow regions. Thanks to the overall uniformity of the premixer in the cross-stream directions, gradients in conditional quantities are small; hence more elaborate ISRN designs do not change results appreciably. In addition, preliminary computations with a range of 30–600 ISRs, using either uniform or nonuniform spacing in all directions, showed that autoignition propensity is not very sensitive to the ISRN design if the spatial resolution of autoignition location (concerning low-temperature or high-temperature) is not of particular interest. Nevertheless, special attention should be given to the size of ISRs placed close to fuel film injection location into the air stream, since conditional scalars may evolve considerably if the residence time in these ISRs exceeds a certain value.

4 Results and Discussion

4.1 Overall Scope. The primary outcome of the present approach is the computation of conditional reacting scalars, such as temperature and mass fractions of species considered to be autoignition precursors, which are allowed to evolve in mixture fraction space until convergence is attained. Autoignition propensity and its sensitivity to operating conditions can be assessed by close examination of the statistically-steady conditional scalars in addition to the time-averaged unconditional ones.

An analysis in mixture fraction space is first conducted in Sec. 4.2, which may be considered similar to analyses performed in mixing layers (e.g., see Refs. [36,37]) or canonical flows (e.g., see Ref. [4,38]) since autoignition propensity in either laminar or turbulent situations is qualitatively similar when expressed in

terms of the mixture fraction [3]. However, the evolution of mean (unconditional) scalars, i.e., $\langle\phi\rangle$ as opposed to its conditional counterpart $Q_\phi \equiv \langle\phi|\eta\rangle$ for a scalar ϕ, is also indispensable in the estimation of autoignition propensity. As dictated by Eq. (7), the evolution of a mean scalar is a result of both its conditional distribution and the local mixture fraction PDF, i.e., the probability of finding a particular $\langle\phi|\eta\rangle$ value locally, which here originated from an inert LES. In other words, scalars conditioned on the mixture fraction are aimed to indicate the likelihood of finding isolated autoignition or flame kernels within the premixer, the appearance of which is also dictated by the statistical behavior of the mixture fraction (e.g., as per its mean and variance). The above will be further elucidated in Secs. 4.3 and 4.4 when focusing on the evolution of the unconditional and spatially-integrated temperature and their sensitivity to operating conditions.

4.2 Analysis of Mixture Fraction Space. For demonstration purposes, the typical behavior of the conditional temperature and selected species is shown in Fig. 4. The reference pressure and temperatures are selected for this example, with the fuel being 10% (v/v) DME and 90% CH_4. Each curve corresponds to a different location within the premixer, marked by a flow coordinate, s, considered zero for the first ISR (found in the vicinity of the fuel injection point) and reaching its maximum at the last ISR (toward the premixer exit).

At $s = 0$, the temperature distribution corresponds to inert mixing between the hot air ($\eta = 0$) and cold fuel ($\eta = 1$) streams, imposed at the inlet of the first ISR. While mixing occurs toward higher s and the time of flight to this location increases, fuel is consumed first by small amounts (here only the DME component is shown) and the temperature increases slightly, followed by a thermal runway, which eventually leads to autoignition at $s/s_{max} \approx 0.25$. A sudden increase in temperature is observed at this location, establishing a flame at the stoichiometric mixture fraction, indicated by the high value of $\langle T|\eta_{st}\rangle$ (upward-pointing triangle) compared to the reference temperature $T_{ox,ref}$. Up to the establishment of the flame, which may be defined as a high-temperature autoignition event, pre-ignition radicals (e.g., $CH_3OCH_2O_2$ in Fig. 4(*c*) and H_2O_2 in Fig. 4(*d*)) are formed which, together with the fuel, are rapidly consumed in regions of high temperature. Note, for example, the absence of the H_2O_2 on the rich side of the stoichiometric mixture fraction at the location $s/s_{max} = 0.25$. Transport in physical space (terms $\mathcal{T}_1$ and $\mathcal{T}_2$ in Eq. (6)) and micromixing ($\mathcal{T}_3$) can propagate the flame further downstream and lead to the consumption of radicals in neighboring mixture fractions, which might have a non-negligible probability.

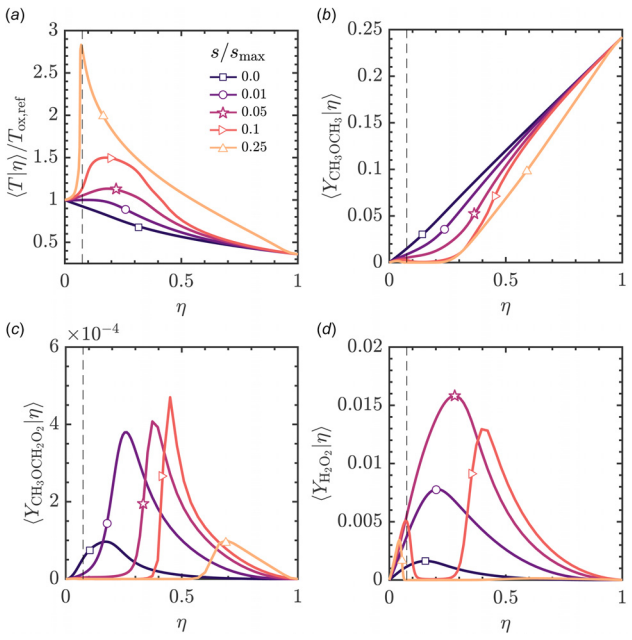

Fig. 4 Mixture fraction space distributions of temperature and mass fraction of selected species at various locations within the premixer, denoted by a flow coordinate, operating at reference pressure and temperature conditions with 10% DME in the fuel mixture. The dashed line indicates the stoichiometric mixture fraction.

High-temperature autoignition in mixture fraction space is of particular interest since it can be a forewarning of flame growth and stabilization with catastrophic consequences to a premixer used in practice. However, note that $\langle T\rangle \gg T_{ox,ref}$ is not always a necessity even if $\langle T|\eta\rangle \gg T_{ox,ref}$, as discussed in Sec. 4.1. The formation of a cool flame is also of particular importance in this configuration. Due to the low-temperature reactivity of DME at high pressure, a cool flame ought also to be established prior to the formation of a hot flame (e.g., see Ref. [5] for a recent review on the topic). The transition to the cool flame may be defined as a low-temperature autoignition event that occurs soon after the fuel is introduced to the domain and is responsible for the initial thermal runway and accumulation of precursors. This may be explained by the short induction times (and by extension, the induction length) needed for low-temperature chemical reactions at high pressure (e.g., see Ref. [39] for examples with homogeneous autoignition) and the influence of the high SDR (intense micromixing) which promotes the diffusion of radicals across a wide range of mixture fractions.

The low-temperature autoignition event is evident from the initial formation of pre-ignition radicals (see square and circle symbols in Figs. 4(*c*) and 4(*d*)). It is noteworthy that these radicals preferentially form at a mixture fraction separated from the stoichiometric. In the absence of hydrodynamic stretch, this formation typically occurs around the most reactive mixture fraction, which in Fig. 3 was shown to be $\xi_{mr} \approx 0.1$ and larger than the stoichiometric. In Fig. 4, the location of the first kernel is still found in a fuel-rich zone but differs from ξ_{mr}. As for the short induction time, the location of the first kernel is also mostly attributed to diffusion in mixture fraction space, consistent with observations from direct numerical simulations (DNS) featuring DME combustion at high pressure and temperature [37,40,41]. The DNS results indicated the action of mixing in promoting low-temperature autoignition and the existence of diffusively-supported cool flames that can propagate to mixture fractions different from the most reactive. For simulation approaches to accurately describe this ignition process, an accurate balance between reaction, transport, and diffusion have to be achieved, posing important modeling challenges [40]. The ISRN approach includes these phenomena in the current initially nonpremixed system, as is the case for all approaches based on the foundation of CMC theory (e.g., see [3,4,29,42]).

Furthermore, alongside low- and high-temperature chemistry, intermediate-temperature chain-branching reactions are taking place which can lead to the formation of a multi-stage warm flame between cool and hot flame [5,39,43–46]. Alternatively, the transition from inert conditions to high-temperature autoignition may occur at more than two stages (low- and high-temperature autoignition) which is typically the case for hydrocarbon fuels (e.g., see Refs. [36,37,47]). The multi-stage autoignition behavior at the investigated conditions can become more evident by closer inspection of the scalar evolution at particular mixture fraction values. Figure 5(*a*) shows the evolution of $\langle T|\eta_{mr}\rangle$ and $\langle T|\eta_{st}\rangle$ (where $\eta_{mr} = \xi_{mr}$ and $\eta_{st} = \xi_{st}$) as a function of the flow coordinate for various levels of DME. For the example of Fig. 4, where DME constitutes 10% of the mixture, strong gradients in temperature may be observed in the vicinity of $s = 0$ (first-stage or low-temperature autoignition), at $s/s_{max} \approx 0.1$ (second-stage) and at $s/s_{max} \approx 0.25$ (third-stage) with the latter leading to a hot flame.

Several metrics can be used to demarcate first- and second-stage ignition events instead of using the temperature since it is

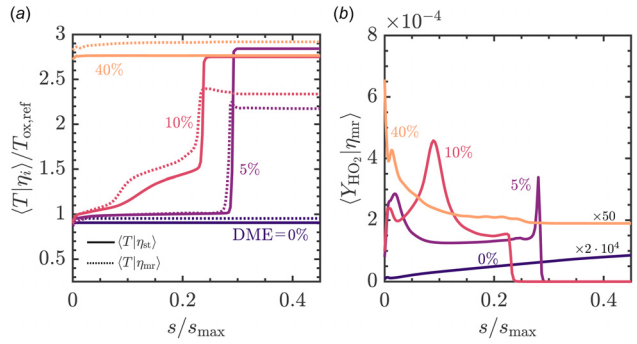

Fig. 5 Evolution of (*a*) temperature and (*b*) HO_2 conditioned on selected mixture fractions a function of the premixer flow coordinate. The premixer operates at the reference conditions with the volume composition of DME in the fuel mixture indicated for each curve. In (*b*), a multiplier has been applied to the 0% and 40% curves.

too distributed to define ignition location clearly. For example, the heat release rate or a reaction rate can be used and also combined with the unconditional value of radicals, such as OH [1]. Another suitable method may be to track pre-ignition radicals conditioned to a particular mixture fraction value, as shown, for example, in Fig. 5(*b*) for the case of HO_2. It is not clear which mixture fraction value is most appropriate for the dual fuel mixture studied here, but this may be elucidated in the future via the help of mathematical tools such as Computational Singular Perturbation (CSP) [48] and the focus on a range of canonical configurations. Although the use of the most reactive mixture fraction as the value of interest might not be fully justified, the evolution of $\langle Y_{HO_2}|\eta_{mr}\rangle$ as a function of s/s_{max} may still be reliably used to estimate the autoignition event location. This is possible by tracking the locations of the peaks, and by extension constructing an autoignition propensity metric to rank various premixer designs. Even in the absence of high-temperature autoignition as is the case of pure CH_4 fuel (DME = 0%) in Fig. 5, the total value of $\langle Y_{HO_2}|\eta_{mr}\rangle$ at the premixer exit could be utilized for premixer ranking, since a higher accumulation of pre-ignition radicals typically indicates higher autoignition propensity when transitioning to more reactive conditions. In the limit of very reactive conditions, as is the case of 40% DME in the fuel in the studied conditions, the demarcation of multi-stage autoignition is not necessary since results indicate the presence of a hot flame in mixture fraction space from the first ISR. Although a much finer resolution in the ISR spacing would show the temperature increase and the overlap between low- and high-temperature autoignition more clearly soon after fuel is introduced to the premixer, this is not strictly necessary for a quick estimation of autoignition propensity. Any ISR spacing could clearly indicate the formation of autoignition kernels along the whole premixer (e.g., see Ref. [6] for the case of a single ISR) and the high probability of flame stabilization at these reactive conditions, as also observed by Jella et al. [1]. For less reactive mixtures, e.g., 5% DME in Fig. 5, multi-stage autoignition may not be as prominent due to the absence of considerable thermal runway; however, peaks in pre-ignition radicals can still show the progress of low-temperature reactions, and consequently the onset to high-temperature autoignition.

4.3 Analysis in Physical Space. As discussed in Sec. 4.1, the evolution of reacting scalars in the premixer is a result of both their conditional distributions and the local mixture fraction PDF, with the first originating from the ISRN computation and the latter from an inert flow computation. To further analyze the statistically-steady autoignition propensity, Eq. (7) may be utilized to extract mean quantities at a particular point in physical space. Having access to the mixture fraction PDF, modeled based on the mean mixture fraction and its variance (both accessible in the whole simulation domain), three-dimensional distributions of temperature and radicals may be computed.

Figure 6 shows typical fields of the unconditional temperature and selected unconditional radicals for two levels of DME in the fuel when the same conditions as in Figs. 4–5 are considered. At 10% DME (left column of Fig. 6), the nondimensionalised temperature takes values above 1 indicating the presence of

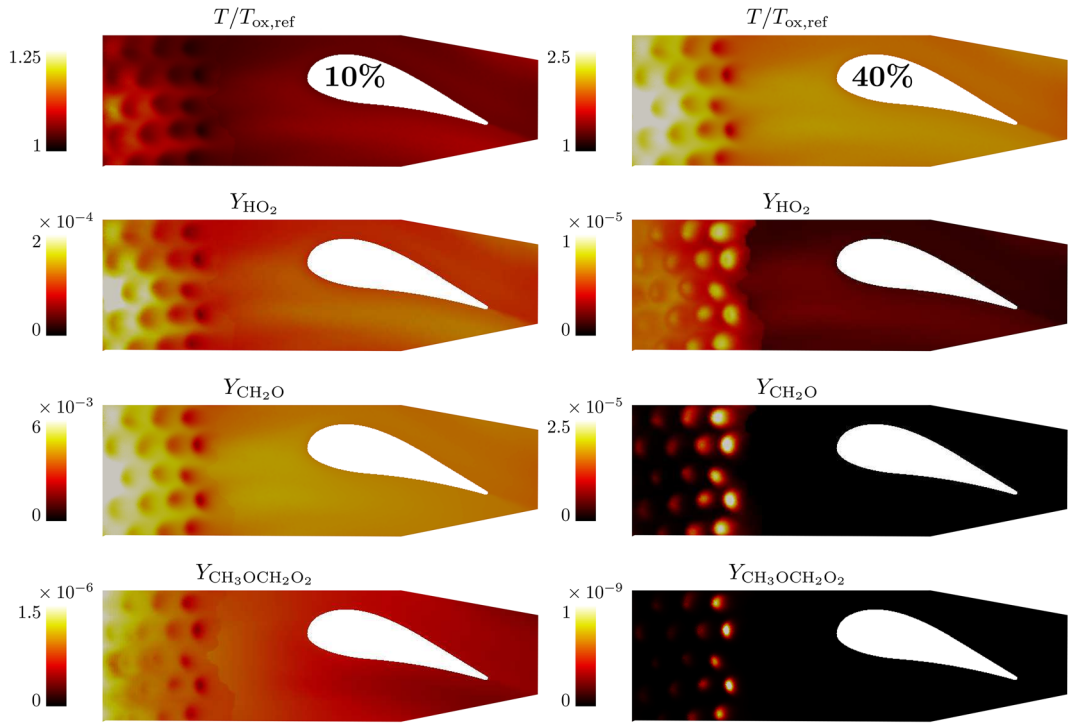

Fig. 6 Mean unconditional fields of temperature and selected radicals in a section of the investigated premixer at the reference conditions with DME = 10% (left) and DME = 40% (right)

exothermic reactions. The radical species HO_2, CH_2O, and CH_3O-CH_2O_2 which are important pre-ignition precursors, appear to rapidly increase in the vicinity of the fuel injection side (left edge), then decrease downstream and finally converge to an almost (spatially) uniform value toward the premixer exit (right edge). "Black spots" at this condition indicate the action of the air jets and the dominance of very lean mixtures, where autoignition reactions do not occur. The analysis of the previous section underlined the presence of multi-stage autoignition for the 10% DME condition shown in Fig. 6. Although high-temperature autoignition was observed in mixture fraction space, it is evident that the premixer is not fully lit but sustains a lower-temperature flame. Due to the intense mixing in the premixer and the transition of the mixture fraction PDF to a Dirac-type distribution toward the premixer exit (see also Fig. 3), the probability of finding hot kernels (in other words, mixture fractions with high temperature, e.g., ξ_{st}) becomes lower toward the premixer exit. Consequently, the mean temperature must decrease.

The above is in contrast with the 40% DME condition (right column of Fig. 6), where the premixer is fully ignited ($T/T_{ox,ref} \gtrsim 2$). Although this behavior is highly undesirable and should be avoided in practice, it is here intended as a means to show the robustness of the premixer to autoignition. Major differences are found compared to the 10% DME case. Due to the high temperature in the domain, radical species are characterized by a smaller magnitude and rapid consumption after the last row of air jets, whereas the local action of the air jets is shown by the "yellow spots". Since the most reactive mixture fraction at this condition is on the lean side of the stoichiometric value (see Fig. 3), autoignition kernels preferentially form in lean mixture fractions (but not necessarily equal to ξ_{mr}), here located in the vicinity of the air jets.

In the aforementioned examples, locations characterized by high radical concentrations may be considered the most susceptible to autoignition. Their prominence and sensitivity to DME are in good agreement with the observations of Jella et al. [1] who conducted a reacting CFD analysis of the same premixer. Although the agreement can only be considered qualitative since the analysis was primarily based on chemical explosive modes and not through pre-ignition radicals, it underlines the usefulness and promise of the ISRN approach in estimating (multi-stage) autoignition propensity.

4.4 Evolution of Spatially-Integrated Scalars. Furthermore, the results of Fig. 6 can be substantiated by appropriate spatial integration. Since conditional averages were found to vary little in the cross-stream directions, also justifying the choice of an ISRN in series (see Sec. 2.2), spatial averaging in directions normal to the flow coordinate can be used to facilitate comparisons between operating conditions. The ISRs are already a function of the flow coordinate, therefore a spatially-integrated mean scalar may be calculated based on:

$$\phi^{**} \equiv \frac{\int_V \bar{\rho} Q_\phi P_\eta dV'}{\rho^{**} V P_\eta^{**}} = \int_0^1 Q_\phi P_\eta^{**} d\eta \tag{8}$$

Figure 7 shows the evolution of spatially-integrated mean scalars as a function of the flow coordinate, similar to what was analyzed previously in the two-dimensional section of the premixer. In addition to 10% DME (magenta) and 40% DME (orange) curves where autoignition and the formation of a low-temperature (10% DME) and high-temperature (40% DME) are evident, results are shown for a case of pure CH_4 fuel. It is apparent that a change in the oxidizer temperature by 40 K is not enough to lead to autoignition. The initial increase in T^{**} is a mere result of mixing between the cold fuel and air at temperature $T_{ox,ref}$. However, the progress of the underlying chemical reactions may be appreciated by the observed build-up of CH_2O and HO_2 toward the premixer exit. The effect of the oxidizer temperature is also not

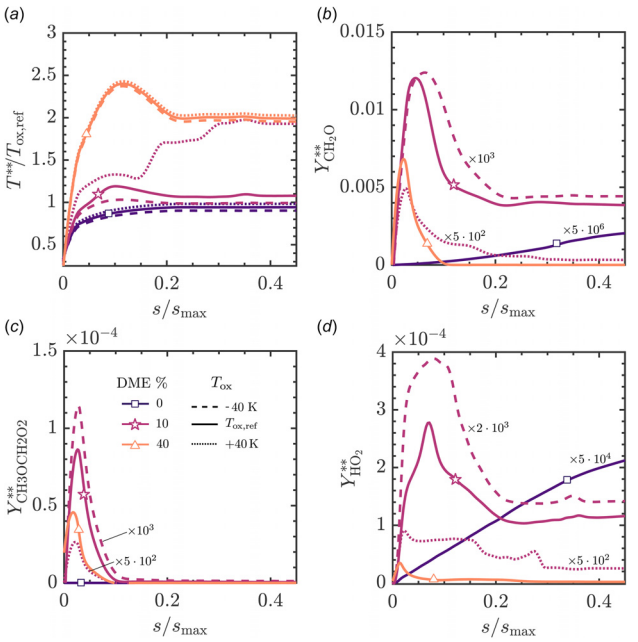

Fig. 7 Evolution of spatially-integrated temperature and selected radicals as a function of the premixer flow coordinate at the reference pressure and fuel temperature. The multipliers used for the scaling of radicals in (*b*)–(*d*) are indicated next to the respective curves.

prominent in the case of 40% DME. As was previously shown in the mixture fraction space analysis of Sec. 4.2, high-temperature autoignition occurs almost instantaneously, leading to the establishment of a hot flame in conserved scalar space. This event appears not to be affected by a decrease in oxidizer temperature. A similar lack of sensitivity to the oxidizer temperature could also be observed in the absence of transport and hydrodynamic stretch effects given that autoignition preferentially occurs at rich conditions, hence temperatures far smaller than the oxidizer's. This condition could be considered equivalent to having a homogeneously rich mixture at an initial temperature within the negative temperature coefficient (NTC) regime [5], although care is needed when comparing premixed and nonpremixed systems. The distribution of T^{**} versus the flow coordinate in the premixer may then be explained from the evolution of the mixture fraction PDF. As autoignition has already occurred and high temperatures are present in mixture fractions around the stoichiometric, the probability of finding those values in the premixer increases as air–fuel mixing progresses, and the mean mixture fraction decays. The temperature reaches a maximum and then decreases to a plateau as the mean mixture fraction decays further toward the well-mixed value, leaner than the stoichiometric (see Sec. 3). The plateau region, which may be observed under all conditions, corresponds to a convergence of the mean mixture fraction. However, note that mixing may be practically not complete since considerable fluctuations around the mean may still be present, which typically take longer to decay (not shown).

The oxidizer temperature predominantly influences the case with 10% DME fuel, which is the most affected by the interplay between low-, intermediate- and high-temperature reactions among all investigated fuel mixtures. The nonmonotonic change in temperature when the oxidizer temperature increases by 40 K results from the mixture fraction PDF, which evolves simultaneously with conditional reacting scalars, subject to multi-stage autoignition as substantiated by the mixture fraction space analysis. The spatially-integrated radical evolution may also reflect the evolution of the temperature. All radicals rapidly accumulate at the start of the premixer ($s \to 0$) and are consequently consumed after the first-stage autoignition is complete. Note, for example,

the more narrow distribution of the $CH_3OCH_2O_2$ radical, which can be used to demarcate the first-stage autoignition location and the onset of the cool flame. Further downstream, CH_2O and HO_2 show a little increase followed by further consumption at $s/s_{max} \approx 0.2$ where a warm flame is established. High-temperature autoignition occurs at $s/s_{max} \approx 0.25$, consistent with the evolution of the conditional values in Figs. 4–5.

The sensitivity of this condition to air temperature is vital for premixer design and operation. As discussed by Iavarone et al. [6], perturbations to influential variables such as temperature may be responsible for rare autoignition events, so that autoignition risk may not be apparent by examination of the nominal operating conditions alone. Thanks to its low computational cost, the ISRN approach may be integrated into new stochastic analysis frameworks (e.g., see Refs. [6,22,49]) that aim to quantify autoignition risk based on a modification to the boundary conditions used in the premixer. For example, if the operating air temperature follows a normal distribution with a standard deviation of $\sigma = 10$ K, then the perturbation of 40 K in Fig. 7 corresponds to $4 \cdot \sigma$, which has a non-negligible probability. Since many simulations would be needed to describe the probability distributions of perturbed variables accurately, the ISRN method is ideal as it can remove the need for many expensive CFD simulations. The computational cost aspects will be further discussed in the following.

4.5 Computational Considerations. The method is computationally very efficient, as previously reported in Refs. [10,11,20]. The mixing field is precalculated, and only a subset of processes is solved at each time-step; hence the computational time is drastically minimized compared to a detailed reacting CFD simulation. With either RANS or LES, inert CFD simulations are routinely performed in the industry and academia and necessitate reasonable computational resources available to most CFD engineers. In the current setup, the total computational time is of the order of 3 h, necessary to reach convergence on one node (32 MPI processes) of an Intel Xeon Skylake supercomputer (Cambridge CSD3). This equates to a total computational cost of 96 CPUh per simulation. Of course, similar performance can also be achieved in a modern multicore workstation, but it might be limited by the available computer memory necessary to process the underlying CFD computation and the total number of scalars.

Faster runtimes than the one reported here may be easily attained as the total runtime scales inversely with the number of total MPI processes. For a generally low number of reactors in the order of $O(1000)$, which is more than adequate to describe autoignition propensity (see related comments in Sec. 3), only slight computational efficiency losses have been observed with the current implementation, even when one processor is used per ISR. Experience with soot modeling and complex chemical mechanisms [10,11] has also shown that the computational penalty of switching to a larger and stiffer chemical mechanism is proportional to the penalty observed in simpler solvers, used, for example, for transient flamelet calculations.

5 Summary and Conclusions

A novel approach using incompletely stirred reactor network (ISRN) modeling to estimate autoignition propensity in aeroderivative premixers has been presented. As a postprocessing step on a nonreacting CFD solution, the approach considers the evolution of statistically-steady conditional reacting scalars, such as temperature and pre-ignition radicals, with the conditioning performed on the mixture fraction. By examining the conditional averages and their time-averaged unconditional counterparts, autoignition propensity and its sensitivity to operating conditions can be closely evaluated. The reacting scalars are computed separately from the flow, enabling the use of complex chemical mechanisms and previously elusive parametric analyses at a moderate computational cost. The method was applied to the time-averaged inert LES fields of an experimental premixer operating at highly reactive conditions and with a dual fuel mixture of methane and dimethyl ether. The analysis underlined the prominence of multistage autoignition within the premixer, strongly influenced by the reactivity of DME and the effects of mixing and turbulent transport. Autoignition propensity observables proved consistent with a previous analysis using reacting CFD, indicating the suitability of the ISRN in describing the ignition processes in initially nonpremixed systems such as gas turbine premixers. The choice of various autoignition metrics that combine the effects of mixing and chemical reactions was further examined to facilitate future premixer designs. The present modeling approach may also be viewed as an extendable framework that can incorporate mathematical tools such as CSP algorithms to describe the underlying autoignition dynamics better [48] and uncertainty quantification methods to perform stochastic analysis and quantify rare autoignition risk [22,35].

Funding Data

- Siemens Energy (Funder ID: 10.13039/501100015664).

Nomenclature

A = area
D = diffusion coefficient
D_T = turbulent diffusivity
N = scalar dissipation rate (SDR)
$\dot{m}$ = mass flow rate
$O(\epsilon)$ = indicates a function of the same order as ϵ
P = mixture fraction probability density function (PDF)
Q = conditional mean (expectation) of reactive scalar
s = flow coordinate
Sc = Schmidt number
T = temperature
t = time
$\mathbf{u}$ = velocity vector
V = volume
Y_α = mass fraction of species α
$\mathcal{F}$ = face index
$\mathcal{T}$ = equation term
Δ = filter width
ϵ = a small number
η = sample space variable of mixture fraction
μ = molecular viscosity
ξ = mixture fraction
ρ = mass density
σ = standard deviation
$\dot{\omega}_\alpha$ = chemical source term of species α
$(\cdot)_i$ = i-th stream indicator
$\cdot_f$ = based on the fuel stream
$\cdot_{in}$ = inlet
$\cdot_{max}$ = maximum
$\cdot_{mixed}$ = defined at the well-mixed condition
$\cdot_{mr}$ = defined at the most reactive condition
$\cdot_{out}$ = outlet
$\cdot_{ox}$ = based on the oxidizer stream
$\cdot_{ref}$ = reference
$\cdot_{sgs}$ = defined at the sub-grid scale

$\cdot_{st}$ = defined at the stoichiometric condition
$\cdot_{\eta}$ = varying in mixture fraction space
$\tilde{\cdot}$ = Favre-filtered
$||\cdot||$ = vector magnitude
$\cdot^{**}$ = core averaged
$\cdot'$ = fluctuation with respect to mean
$''^2$ = sub-grid scale variance
$\bar{\cdot}$ = conventional average
$\langle\cdot\rangle$ = ensemble average
$\langle\cdot|\eta\rangle$ = conditional average

References

[1] Jella, S., Bourque, G., Gauthier, P., Versailles, P., Bergthorson, J., Park, J.-W., Lu, T., Panigrahy, S., and Curran, H., 2021, "Analysis of Auto-Ignition Chemistry in Aeroderivative Premixers at Engine Conditions," ASME J. Eng. Gas Turbines Power, **143**(11), p. 111024.

[2] Scarinci, T., Freeman, C., and Day, I., 2004, "Passive Control of Combustion Instability in a Low Emissions Aeroderivative Gas Turbine," ASME Paper No. GT2004-53767.

[3] Mastorakos, E., 2009, "Ignition of Turbulent Non-Premixed Flames," Prog. Energy Combust. Sci., **35**(1), pp. 57–97.

[4] Stanković, I., Triantafyllidis, A., Mastorakos, E., Lacor, C., and Merci, B., 2011, "Simulation of Hydrogen Auto-Ignition in a Turbulent co-Flow of Heated Air With LES and CMC Approach," Flow, Turbul. Combust., **86**(3–4), pp. 689–710.

[5] Ju, Y., Reuter, C. B., Yehia, O. R., Farouk, T. I., and Won, S. H., 2019, "Dynamics of Cool Flames," Prog. Energy Combust. Sci., **75**, p. 100787.

[6] Iavarone, S., Gkantonas, S., Jella, S., Versailles, P., Yousefian, S., Mastorakos, E., and Bourque, G., 2022, "Quantification of Autoignition Risk in Aeroderivative Gas Turbine Premixers Using Incompletely Stirred Reactor and Surrogate Modelling," ASME Paper No. GT2022-82931.

[7] Kaluri, A., Malte, P., and Novosselov, I., 2018, "Real-Time Prediction of Lean Blowout Using Chemical Reactor Network," Fuel, **234**, pp. 797–808.

[8] Yousefian, S., Bourque, G., and Monaghan, R. F. D., 2017, "Review of Hybrid Emissions Prediction Tools and Uncertainty Quantification Methods for Gas Turbine Combustion Systems," ASME Paper No. GT2017-64271.

[9] Khodayari, H., Ommi, F., and Saboohi, Z., 2020, "A Review on the Applications of the Chemical Reactor Network Approach on the Prediction of Pollutant Emissions," Aircr. Eng. Aerosp. Technol., **92**(4), pp. 551–570.

[10] Gkantonas, S., Foale, J. M., Giusti, A., and Mastorakos, E., 2020, "Soot Emission Simulations of a Single Sector Model Combustor Using Incompletely Stirred Reactor Network Modeling," ASME J. Eng. Gas Turbines Power, **142**(10), p. 101007.

[11] Gkantonas, S., 2021, "Predicting Soot Emissions with Advanced Turbulent Reacting Flow Modelling," Ph.D. thesis, University of Cambridge, Cambridge, UK.

[12] Smith, N. S. A., 1994, "Development of the conditional moment closure method for modelling turbulent combustion," Ph.D. thesis, University of Sydney, Sydney, Australia.

[13] Mobini, K., 1998, "An investigation of the imperfectly stirred reactor modelling of recirculating combustion flows," Ph.D. thesis, University of Sydney, Sydney, Australia.

[14] Mobini, K., and Bilger, R., 2004, "Imperfectly Stirred Reactor Model Predictions of Reaction in a Burner With Strong Recirculation," Combust. Sci. Technol., **176**(1), pp. 45–70.

[15] Mobini, K., and Bilger, R., 2009, "Parametric Study of the Incompletely Stirred Reactor Modeling," Combust. Flame, **156**(9), pp. 1818–1827.

[16] Klimenko, A., and Bilger, R., 1999, "Conditional Moment Closure for Turbulent Combustion," Prog. Energy Combust. Sci., **25**(6), pp. 595–687.

[17] Gough, A., Mobini, K., Chen, Y.-C., and Bilger, R., 1998, "Measurements and Predictions in a Confined Bluff-Body Burner Modeled as an Imperfectly Stirred Reactor," Symp. (Int.) Combust., **27**(2), pp. 3181–3188.

[18] Trivedi, S., Gkantonas, S., Wright, Y. M., Parravicini, M., Barro, C., and Mastorakos, E., 2021, "Conditional Moment Closure Approaches for Simulating Soot and NOx in a Heavy-Duty Diesel Engine," SAE Paper No. 2021-24-0041.

[19] Gkantonas, S., Giusti, A., and Mastorakos, E., 2019, "Incompletely Stirred Reactor Network Modelling for Soot Emissions Prediction in Aero-Engine Combustors," Proceedings of the International Workshop on Clean Combustion: Principles and Applications, Darmstadt, Germany, Sept. 25–26.

[20] Gkantonas, S., Giusti, A., and Mastorakos, E., 2020, "Incompletely Stirred Reactor Network Modeling of a Model Gas Turbine Combustor," AIAA Paper No. 2020-2087.

[21] Iavarone, S., Gkantonas, S., and Mastorakos, E., 2022, "Incompletely Stirred Reactor Network Modeling for the Estimation of Turbulent Non-Premixed Autoignition," International Colloquium on the Dynamics of Explosions and Reactive Systems (ICDERS), Naples, Italy, June 19–24, Paper No. 51.

[22] Iavarone, S., Gkantonas, S., and Mastorakos, E., 2022, "Stochastic Low-Order Modelling of Hydrogen Autoignition in a Turbulent Non-Premixed Flow," Proc. Combust. Inst., epub.

[23] Markides, C., and Mastorakos, E., 2005, "An Experimental Study of Hydrogen Autoignition in a Turbulent co-Flow of Heated Air," Proc. Combust. Inst., **30**(1), pp. 883–891.

[24] Markides, C. N., 2005, "Autoignition in Turbulent Flows," Ph.D. thesis, University of Cambridge, Cambridge, UK.

[25] Sreedhara, S., Lee, Y., Huh, K. Y., and Ahn, D., 2008, "Comparison of Submodels for Conditional Velocity and Scalar Dissipation in CMC Simulation of Piloted Jet and Bluff-Body Flames," Combust. Flame, **152**(1–2), pp. 282–286.

[26] O'Brien, E. E., and Jiang, T.-L., 1991, "The Conditional Dissipation Rate of an Initially Binary Scalar in Homogeneous Turbulence," Phys. Fluids A: Fluid Dyn., **3**(12), pp. 3121–3123.

[27] Mortensen, M., 2005, "Consistent Modeling of Scalar Mixing for Presumed, Multiple Parameter Probability Density Functions," Phys. Fluids, **17**(1), p. 018106.

[28] Devaud, C. B., Bilger, R. W., and Liu, T., 2004, "A New Method of Modeling the Conditional Scalar Dissipation Rate," Phys. Fluids, **16**(6), pp. 2004–2011.

[29] Wright, Y., Depaola, G., Boulouchos, K., and Mastorakos, E., 2005, "Simulations of Spray Autoignition and Flame Establishment With Two-Dimensional CMC," Combust. Flame, **143**(4), pp. 402–419.

[30] Nicoud, F., and Ducros, F., 1999, "Subgrid-Scale Stress Modelling Based on the Square of the Velocity Gradient Tensor," Flow, Turbulence Combust., **62**(3), pp. 183–200.

[31] Jiménez, C., Ducros, F., Cuenot, B., and Bédat, B., 2001, "Subgrid Scale Variance and Dissipation of a Scalar Field in Large Eddy Simulations," Phys. Fluids, **13**(6), pp. 1748–1754.

[32] Branley, N., and Jones, W., 2001, "Large Eddy Simulation of a Turbulent Non-Premixed Flame," Combust. Flame, **127**(1–2), pp. 1914–1934.

[33] Garmory, A., and Mastorakos, E., 2011, "Capturing Localised Extinction in Sandia Flame f With LES–CMC," Proc. Combust. Inst., **33**(1), pp. 1673–1680.

[34] Sitte, M. P., Turquand d'Auzay, C., Giusti, A., Mastorakos, E., and Chakraborty, N., 2021, "A-Priori Validation of Scalar Dissipation Rate Models for Turbulent Non-Premixed Flames," Flow, Turbul. Combust., **107**(1), pp. 201–218.

[35] Iavarone, S., Gkantonas, S., Giusti, A., and Mastorakos, E., 2021, "Data-Driven Incompletely Stirred Reactor Network Modeling of an Aero-Engine Model Combustor," Proceedings of the 13th International ERCOFTAC Symposium, Rhodes, Greece, Sept. 15–17.

[36] Liu, S., Hewson, J. C., Chen, J. H., and Pitsch, H., 2004, "Effects of Strain Rate on High-Pressure Nonpremixed n-Heptane Autoignition in Counterflow," Combust. Flame, **137**(3), pp. 320–339.

[37] Krisman, A., Hawkes, E. R., Talei, M., Bhagatwala, A., and Chen, J. H., 2017, "A Direct Numerical Simulation of Cool-Flame Affected Autoignition in Diesel Engine-Relevant Conditions," Proc. Combust. Inst., **36**(3), pp. 3567–3575.

[38] Minamoto, Y., and Chen, J. H., 2016, "DNS of a Turbulent Lifted DME Jet Flame," Combust. Flame, **169**, pp. 38–50.

[39] Zhang, H., Hawkes, E. R., Chen, J. H., and Kook, S., 2013, "A Numerical Study of the Autoignition of Dimethyl Ether With Temperature Inhomogeneities," Proc. Combust. Inst., **34**(1), pp. 803–812.

[40] Krisman, A., Hawkes, E. R., Talei, M., Bhagatwala, A., and Chen, J. H., 2016, "Characterisation of Two-Stage Ignition in Diesel Engine-Relevant Thermochemical Conditions Using Direct Numerical Simulation," Combust. Flame, **172**, pp. 326–341.

[41] Jin, T., Luo, K. H., Wang, X., Luo, K., and Fan, J., 2019, "Dynamics of Triple-Flames in Ignition of Turbulent Dual Fuel Mixture: A Direct Numerical Simulation Study," Proc. Combust. Inst., **37**(4), pp. 4625–4633.

[42] De Paola, G., Kim, I. S., and Mastorakos, E., 2009, "Second-Order Conditional Moment Closure Simulations of Autoignition of an n-Heptane Plume in a Turbulent Coflow of Heated Air," Flow, Turbul. Combust., **82**(4), pp. 455–475.

[43] Oshibe, H., Nakamura, H., Tezuka, T., Hasegawa, S., and Maruta, K., 2010, "Stabilized Three-Stage Oxidation of DME/Air Mixture in a Micro Flow Reactor With a Controlled Temperature Profile," Combust. Flame, **157**(8), pp. 1572–1580.

[44] Yamamoto, A., Oshibe, H., Nakamura, H., Tezuka, T., Hasegawa, S., and Maruta, K., 2011, "Stabilized Three-Stage Oxidation of Gaseous n-Heptane/Air Mixture in a Micro Flow Reactor With a Controlled Temperature Profile," Proc. Combust. Inst., **33**(2), pp. 3259–3266.

[45] El-Asrag, H. A., and Ju, Y., 2013, "Direct Numerical Simulations of Exhaust Gas Recirculation Effect on Multistage Autoignition in the Negative Temperature Combustion Regime for Stratified HCCI Flow Conditions by Using H2O2 Addition," Combust. Theory Modell., **17**(2), pp. 316–334.

[46] Sarathy, S. M., Tingas, E.-A., Nasir, E. F., Detogni, A., Wang, Z., Farooq, A., and Im, H., 2019, "Three-Stage Heat Release in n-Heptane Auto-Ignition," Proc. Combust. Inst., **37**(1), pp. 485–492.

[47] Westbrook, C. K., 2000, "Chemical Kinetics of Hydrocarbon Ignition in Practical Combustion Systems," Proc. Combust. Inst., **28**(2), pp. 1563–1577.

[48] Tingas, E. A., Kyritsis, D. C., and Goussis, D. A., 2015, "Autoignition Dynamics of DME/Air and EtOH/Air Homogeneous Mixtures," Combust. Flame, **162**(9), pp. 3263–3276.

[49] Yousefian, S., Bourque, G., and Monaghan, R. F. D., 2019, "Uncertainty Quantification of NOx and CO Emissions in a Swirl-Stabilized Burner," ASME J. Eng. Gas Turbines Power, **141**(10), p. 101014.